Matter

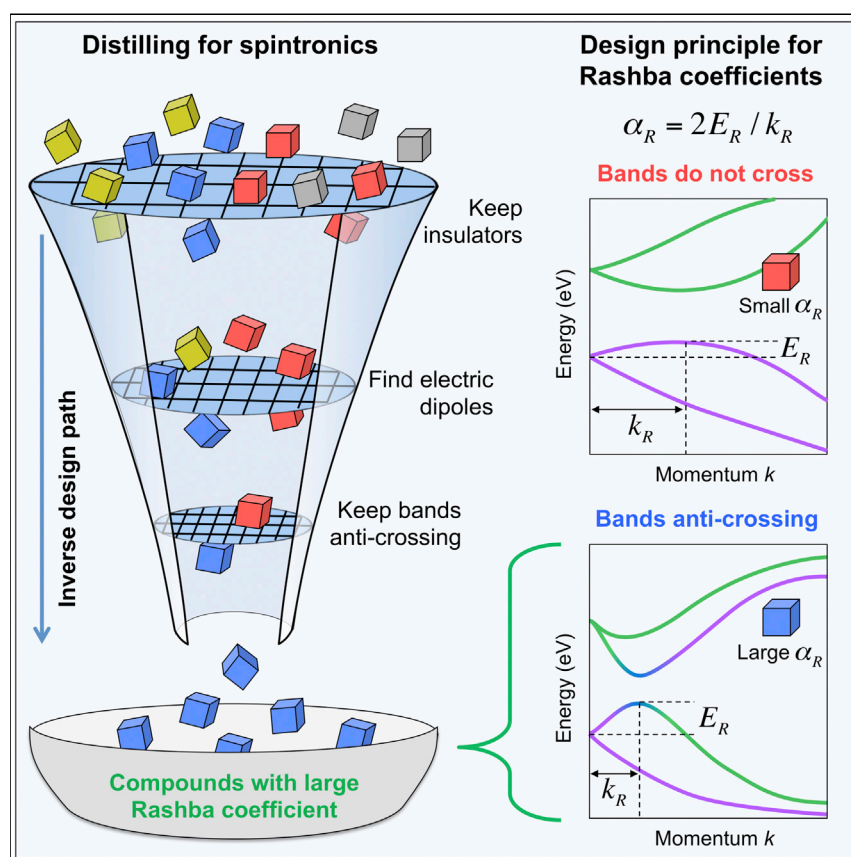### Article

The Rashba Scale: Emergence of Band Anti-crossing as a Design Principle for Materials with Large Rashba Coefficient

Distilling for spintronics

Design principle for Rashba coefficients

$$\alpha_R = 2E_R / k_R$$

Keep insulators

Find electric dipoles

Keep bands anti-crossing

Inverse design path

Compounds with large Rashba coefficient

Bands do not cross

Energy (eV)

Small α_R

E_R

k_R

Momentum k

Bands anti-crossing

Energy (eV)

Large α_R

E_R

k_R

Momentum k

Carlos Mera Acosta, Elton Ogoshi, Adalberto Fazzio, Gustavo M. Dalpian, Alex Zunger

alex.zunger@colorado.edu

HIGHLIGHTS

Uncovering what decides large spin splitting: energy band anti-crossing

Proposing a way to detect band anti-crossing form atomic orbital content

All non-centrosymmetric topological insulators must have large Rashba coefficient

Inverse design uncovers 34 compounds with strong Rashba spin splitting

The generation of spin currents from charge currents forms the basis for a new form (spintronics) of electronics. This, however, requires finding materials capable of having large splitting between their spin bands. Thus far, no hallmark has been known to aid the hunt for such compounds. Using the inverse design approach, we find an unsuspected quantum hallmark—the existence of anti-crossing between energy bands—to be the give-away signal. This enabled identification of 34 compounds with unusually strong spin splitting.

3 **Understanding**
Dependency and conditional studies on material behavior

Article

The Rashba Scale: Emergence of Band Anti-crossing as a Design Principle for Materials with Large Rashba Coefficient

Carlos Mera Acosta,[1,2] Elton Ogoshi,[2] Adalberto Fazzio,[3] Gustavo M. Dalpian,[2] and Alex Zunger[1,4,*]

SUMMARY

The spin-orbit-induced spin splitting of energy bands in low-symmetry compounds (the Rashba effect) has a long-standing relevance to spintronic applications and the fundamental understanding of symmetry breaking in solids, yet the knowledge of what controls its magnitude in different materials is difficult to anticipate. Indeed, rare discoveries of compounds with large Rashba coefficients are invariably greeted as pleasant surprises. We advance the understanding of the "Rashba Scale" using the "inverse design" approach by formulating theoretically the relevant design principle and then identifying compounds satisfying it. We show that the presence of energy band anti-crossing provides a causal design principle of compounds with large Rashba coefficients, leading to the identification via first-principles calculations of 34 rationally designed strong Rashba compounds. Since topological insulators must have band anti-crossing, this establishes an interesting cross-functionality of "topological Rashba insulators" that may provide a platform for the simultaneous control of spin splitting and spin polarization.

INTRODUCTION

Spintronics aims at generation, detection, and control of the spin degrees of freedom with the relevant functionalities being generally based on the magneto-electrical generation of spin-polarized states.[1–3] Rashba noted in 1959[4,5] that when an asymmetric electric potential breaks inversion symmetry, spin-orbit coupling (SOC) creates an effective magnetic field that leads to spin-split and polarized bands. The magnitude of the effect[6,7] is given by the ratio between the spin splitting E_R and the momentum offset k_R, that is, $\alpha_R = 2E_R/k_R$. Strong and weak Rashba effects are defined by the measured or density functional theory (DFT)-calculated magnitude of the Rashba coefficient. Symmetry wise, the existence of a Rashba effect of arbitrary magnitude α_R requires a compound with non-centrosymmetric structures having local electric dipoles induced by polar atomic sites that add up over the unit cell to a non-zero.[8,9] Despite the fact that large Rashba effect is needed for facile spintronic generation and detection of spin-polarized states[10–13] as well as for the detection of Majorana fermions,[14,15] the principles determining the magnitude of this functionality ("the Rashba scale") has not been established. Indeed, the discovery of new compounds with large Rashba coefficient (e.g., GeTe [$R3m$],[16,17] BiTeI [$P3m1$],[18,19] and metallic PtBi$_2$ [$P3m1$][20]) is invariably greeted as a pleasant surprise. The few available literature calculations of compounds with significant α_R and the general absence of examples of compounds with weak Rashba effect poses a severe bottleneck to the understanding of the underlying physical factors controlling the trends, as well as to the prospects of advancing effective spintronic technology.

Progress and Potential

Spintronic devices that dissipate far less heat than electronic devices require spin current generation and control, both provided by the Rashba effect. But the discovery of compounds with large Rashba coefficient α_R is rare and greeted as a pleasant surprise. We establish the existence of anti-crossing between spin energy bands as a viable design principle for identifying compounds with large α_R. We use this principle in quantum mechanical calculations as a filter, delineating 165 weak Rashba compounds from 34 strong Rashba compounds. Experimental testing of spin splitting in these compounds is called for and might significantly broaden the playing field of spintronics. Surprisingly, this research also uncovered a new type of cross-functionality combining two hitherto separate functionalities: topological insulators (having surface states resilient to passivation) with Rashba spin splitting. Such topological Rashba insulators might offer a platform for robust surface spin currents.

We show in this paper that the magnitude of Rashba coefficients in different compounds is not well correlated with the magnitude of the SOC, and that the hallmark of strong Rashba coefficient is the appearance of energy band anti-crossing of the Rashba split bands. This has a few immediate consequences: First, because all topological insulators must have band anti-crossing, we show that all non-centrosymmetric topological insulators having non-zero electric dipole (i.e., topological insulators [TIs] that can have a Rashba effect) must be strong Rashba compounds. This provides a causal physical explanation for previous occasional observations of TIs having large Rashba coefficients[21–24] and establishes a new cross-functionality: topological Rashba insulators (TRIs). Searching current databases of TI compounds[25–27] for TI members that are also non-centrosymmetric with non-zero electric dipole predicts a few TRIs such as Sb_2Te_2Se and TlN with calculated large α_R of 3.88 eVÅ and 2.64 eVÅ in the valence bands, respectively. Second, we show that the anti-crossing theory of the Rashba scale can be used to identify new strong Rashba compounds by a different route—starting from known non-centrosymmetric structures—and identify those that also have anti-crossing bands. This approach led to identification of 34 previously synthesized strong Rashba compounds, including the already known GeTe and BiTeI, as well as compounds that have been previously synthesized but were unappreciated as Rashba compounds, let alone as strong Rashba compounds, such as BiTeCl ($P6_3mc$), PbS ($R3m$), and $K_2BaCdSb_2$ ($Pmc2_1$) with Rashba coefficients of 4.5, 4.6, and 5.3 eVÅ, respectively. Additionally, we also identify 165 weak Rashba compounds with Rashba parameter smaller than 1.2 eVÅ and Rashba spin splitting (RSS) larger than 1 meV (see Supplemental Information I). We hope that these predictions will be tested experimentally.

The theory above follows an inverse design approach: it predicts target properties based on physically motivated models that directly connect the existence of the desired property with an explicit physical mechanism.[28–31] Searching of specific realizations of such materials is then performed by first-principles calculations, looking for the above-established metric of the physical mechanism in real materials. This is different from an exhaustive search data-directed approach in which the discovery of materials with a given functionality is based on high-throughput computation of all (or many) possible combinations of atomic identities, composition, and structures.[32,33] This is also different from traditional machine learning, in that inverse design relies on the use of an explicitly causal physical mechanism rather than on the correlation of, say, atomistic features with the target functionality.[34–36]

The main accomplishments of the current work are: (1) the development of the definition of the Rashba scale: all materials with larger than certain value α_R have band anti-crossing, and below that threshold none has band anti-crossing; (2) the demonstration of how anti-crossing bands can be identified form the atomic orbital contribution to the band structure; (3) the establishment of TRIs; (4) the inverse design of 34 strong Rashba compounds and 165 weak Rashba compounds based on the proposed theory, i.e., the anti-crossing as design principle for strong Rashba materials. The advance offered by this establishment of a bridge between electronic structure (i.e., band anti-crossing) and the "Rashba scale" may offer a platform for the exploration of other phenomena potentially hosted by Rashba compounds, e.g., superconductivity and Majorana fermions.

RESULTS

Shortcomings in the Current Understanding of Trends in the Rashba Scale

To discuss trends in the Rashba scale, Figure 1A presents DFT-calculated Rashba coefficients (see Experimental Procedures for details of calculations) of 125
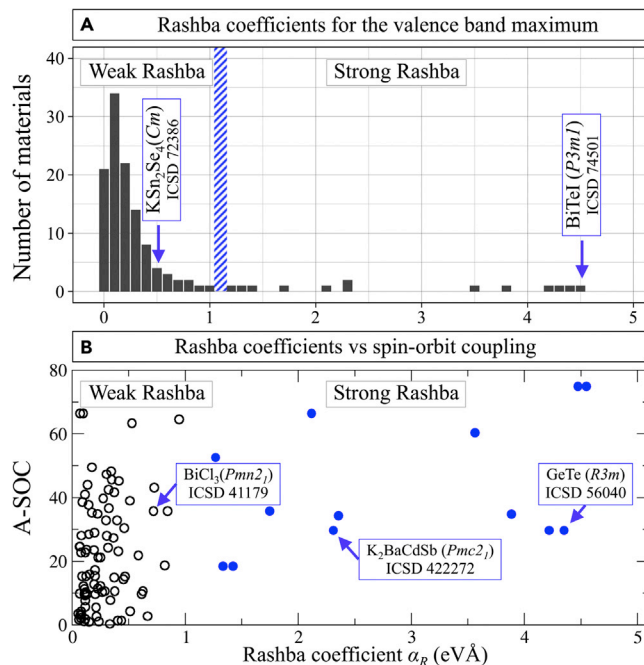
[1]Renewable and Sustainable Energy Institute, University of Colorado, Boulder, CO 80309, USA

[2]Center for Natural and Human Sciences, Federal University of ABC, Santo Andre, SP, Brazil

[3]Brazilian Nanotechnology National Laboratory CNPEM, Campinas, SP 13083-970, Brazil

[4]Lead Contact

*Correspondence: alex.zunger@colorado.edu

https://doi.org/10.1016/j.matt.2020.05.006

Figure 1. Distribution of the Magnitude of Rashba Coefficients

(A) DFT calculated (see Experimental Procedures for details) Rashba coefficients for the valence band maximum of 125 compounds. The plot reveals a general delineation into "strong" (illustrated by BiTeI) and "weak" (illustrated by KSn_2Se_4) Rashba coefficients. Their Inorganic Crystal Structure Database (ICSD) code and space group are indicated in Table 2 and Supplemental Information I, respectively. The blue hatched area indicates the general delineation.

(B) Rashba coefficients versus an average of the atomic spin-orbit coupling weighted by the composition (A-SOC) for the valence band maximum of 125 compounds, for weak (unfilled black dots) and strong (filled blue dots) Rashba compounds.

compounds that have larger than 1 meV spin splitting near the valence band maximum. This gives a broader impression of the distribution of the magnitude of the Rashba coefficients than what is currently available from isolated literature calculations. We focus on compounds with intrinsic dipoles ("bulk Rashba effect,"[13] denoted as R-1). We exclude (1) magnetic compounds (no time-reversal-symmetry) in which the Zeeman effect is observed instead,[37,38] (2) surfaces or interfaces induced Rashba effects (the "R-0" effect),[7,39] which require non-bulk symmetry breaking, and (3) centrosymmetric compounds with local sectors that have non-centrosymmetric point groups ("hidden Rashba effect"[8,9] or R-2). Figure 1A shows the existence of a significant range of α_R and a general delineation (marked approximately by the blue hatched lines) into small versus large band edge Rashba effects, which are based on α_R and hereafter referred to as weak versus strong Rashba, respectively.

In the phenomenological Hamiltonian describing the linear-in-k Rashba effect in quasi-two-dimensional (2D) systems,[6,7]

$$H(k) = -\sigma_0 \frac{\hbar^2 k^2}{2m^*} + \alpha_R \left(\sigma_x k_y - \sigma_y k_x \right), \qquad \text{(Equation 1)}$$

the magnitude of the Rashba coefficient α_R is associated with the intrinsic atomic SOC. However, the continuum $k \cdot p$ theory underlying the literature based on Equation (1) does not disclose trends in the magnitude of α_R, for which an atomistic resolution is needed. Indeed, we will show that materials with larger than certain value
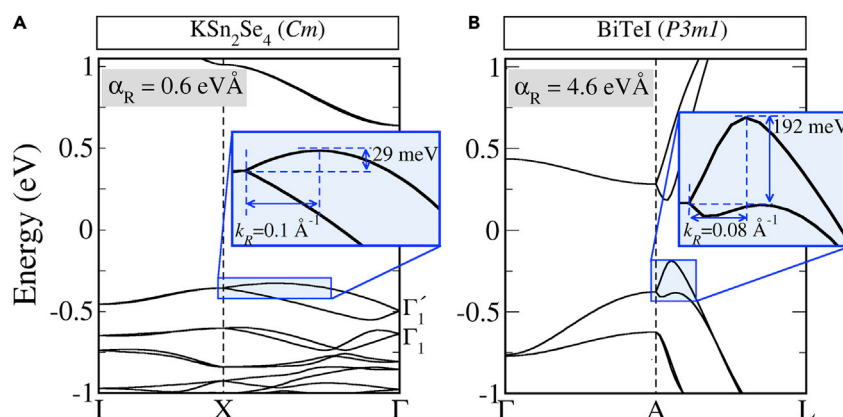
Figure 2. DFT Band Structure Calculations of Prototype Compounds Characterized by Different Band Shapes

(A) Without anti-crossing bands, and (B) with anti-crossing. This results in small (α_R = 0.6 eVÅ) and large (α_R = 4.6 eVÅ) Rashba parameters, respectively. The different band shapes, momentum offset, and Rashba spin splitting are highlighted in the blue insets. In KSn$_2$Se$_4$, the valence bands have the same symmetry representation (Γ_1 and Γ'_1).

α_R have band anti-crossing, and below that threshold none has band anti-crossing. Furthermore, the continuum-like Rashba Hamiltonian of Equation (1) mimics microscopic energy level quantum models only for the specific cases of non-crossing bands.

In three-dimensional (3D) compounds, the bulk Rashba effect can depend on the inter-atomic orbital interaction, hindering the description of this effect by Equation (1) even in planes perpendicular to the electric dipole. Inspection of DFT results in Figure 1 shows, however, that this scaling through SOC is not the whole picture. Figure 1B shows the Rashba coefficient at the valence band maximum (VBM) plotted versus the composition-weighted average of the atomic SOC values (A-SOC) of the respective compounds (taken from Martin[40]). This reveals that for compounds defined as "weak Rashba" (open black circles) there is a generally non-monotonic trend of α_R with A-SOC, making it unlikely to predict a sequence of compounds with monotonic α_R values based on A-SOC alone. Thus, compounds with lower SOC can have larger Rashba coefficients than those with higher SOC. This is illustrated for instance by K$_2$BaCdSb$_2$ (space group $Pmc21$) having large calculated α_R of 2.36 eVÅ for the valence band and 5.25 eVÅ for the conduction band, while having a smaller atomic A-SOC than BiCl3 (space group $Pmn21$) with α_R = 0.72 eVÅ for the valence band and α_R = 0.403 eVÅ for the conduction band.

Role of Orbital Interactions and Band Shapes in Determining the Rashba Scale

The definition of $\alpha_R = 2E_R/k_R$ suggests that a large Rashba coefficient must be a statement of large energy splitting E_R obtained in a short momentum step k_R, whereas small Rashba coefficient necessarily means small energy split achieved in a long wavevector step. Such different dispersion curves are indeed apparent in previous DFT calculations, as illustrated in Figure 2 for the prototypical band shape in BiTeI and KSn$_2$Se$_4$ with Rashba coefficient in the VBM of 4.6 and 0.6 eVÅ, respectively. One notices qualitatively different behaviors of the dispersion shape of the Rashba bands of strong Rashba compounds versus weak Rashba compounds: BiTeI (space group $P3m1$) has a significant bowing of the bands with small momentum offset and large RSS, compared with KSn$_2$Se$_4$ (space group Cm) with its weakly

dispersed band, large momentum offset, and small RSS. These trends translate into large α_R (as in BiTeI) and small α_R (e.g., KSn_2Se_4).

Tight-Binding Model that Allows Continuous Transition between Weak and Strong Rashba Behavior

In establishing whether these characteristic dispersion shapes also have a causal relationship with the magnitude of the Rashba coefficient in a given material (rather than in chemically dissimilar compounds such as KSn_2Se_4 and BiTeI), it would be useful to control the dispersion shapes in the same material. Unfortunately this is not easy to do with DFT since the band shape can strongly depend on the atomic composition, lattice symmetry, and specific orbital interactions. Nevertheless, such shape engineering of band dispersion is readily possible within a tight-binding (TB) model which, however, does not have the additional virtue of material realism. Our strategy is therefore to use a simple TB model that enables transmuting the shape of Rashba band dispersion between the two prototypes of Figure 2, thus establishing what controls large versus small Rashba effects in a toy model, then use this TB identification of a metric in precise and material specific (3D) DFT calculations and observe how this reveals strong versus weak Rashba effects in real compounds. To this end, we constructed a model Hamiltonian including the minimal essential ingredients at play, namely: two orbitals at different sites, opposite effective mass sign, and SOC (t_{soc}). For illustrative purposes, we only consider s- and p_x-orbitals interacting through the hopping term t_{sp}. A detailed description of the effective TB Hamiltonian used here is given in Experimental Procedures.

For the TB parameter set corresponding to no SOC and non-interacting bands, we find, as expected, non-crossing bands (i.e., different on-site energies $\varepsilon_s > \varepsilon_p$) having parabolic shapes with no Rashba effect (Figure 3A). When these bands are allowed to interact (via setting $t_{sp} > 0$) and experience SOC, as in Figure 3B, the emerging Rashba band shapes is typically "small E_R and large k_R", with its small attendant Rashba coefficient. To change qualitatively the dispersion shape to "large E_R and small k_R" one needs to bring the non-interacting bands (shown in Figure 3C) closer to each other, (e.g., by making the on-site energies similar, $\varepsilon_s \approx \varepsilon_p$). Notably, when the non-interacting crossing parabolic bands (Figure 3C) are allowed to experience SOC and interact (Figure 3D), this orbital interaction (of the same magnitude as in Figure 3B) leads to band anti-crossing with large and linear Rashba effect. This also provides a qualitative description of the typical orbital character behavior in band anti-crossing, i.e., the orbital character drastically changes (e.g., form s- to p_x-orbitals in the VBM shown in Figure 3D) as the k-vector changes from smaller to larger values than k_R (Figure 3D). The predicted band shapes in the linear Rashba effect with non-crossing bands (Figure 3B) and with anti-crossing bands (Figure 3D) provide a differentiation between the band dispersion of a weak Rashba compound illustrated by DFT calculation on KSn_2Se_4 (Figure 2A) versus a strong Rashba compound illustrated by DFT calculation on BiTeI (Figure 2B). Thus, band anti-crossing due to band interaction is the deciding factor, within the simple TB model, for the transition between the weak Rashba to the strong Rashba band shape behavior.

The TB model provides insight to the behavior of the classic Rashba Hamiltonian (Equation 1). This classic Rashba Hamiltonian mimics TB only for the specific cases of non-crossing bands: in TB, for non-interacting bands, the diagonal elements of the block diagonal Hamiltonian describe single-orbital bands, leading to the expression $H_p(k) \approx -\sigma_0(t_{pp}a^2k_x^2) + 2at_{soc}^p(\sigma_y k_x)$ for p-orbitals (with $t_{pp} = \varepsilon_p/2$), as shown in Experimental Procedures. Thus, $H_p(k)$ is equivalent to Equation 1 (by taking $t_{pp}a^2 = \hbar^2/2m^*$ and $\alpha_R = 2at_{soc}^p$ for $k_y = 0$). This illustrates that for non-crossing bands, α_R is
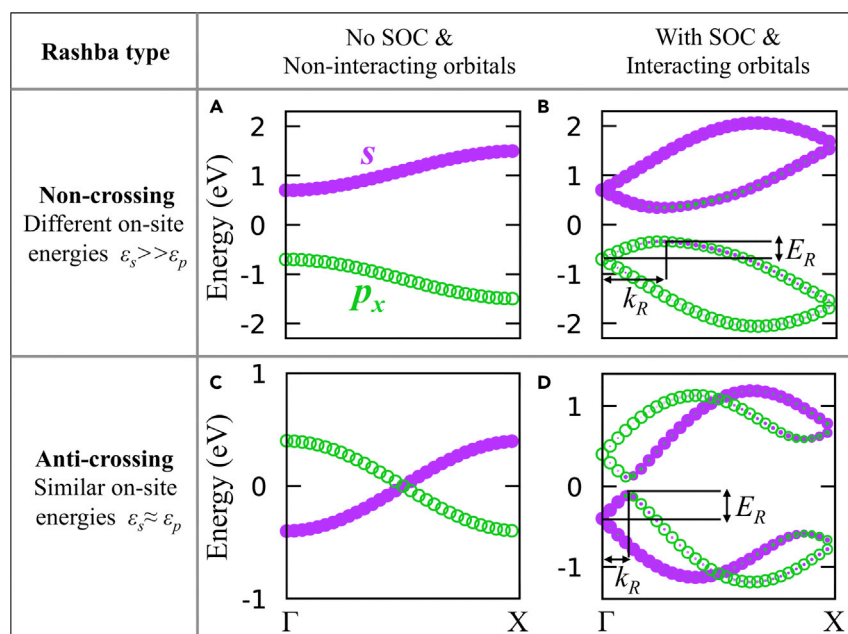
Figure 3. Illustration of the Band-Crossing and Band Anti-crossing in the Rashba Effect

Evolution of the band structure along the line Γ-X for both kinds of Rashba (non-crossing bands [$\varepsilon_s = -\varepsilon_p = 0.55$ eV] and with anti-crossing bands [$\varepsilon_s = -\varepsilon_p = 0$ eV]) for the case of: (A) and (C) no SOC and no inter-orbital coupling sp (t_{sp}); and (B) and (D) SOC (t_{soc}) and inter-orbital interaction. Here, $t_{soc} = 0.4$ eV, $t_{sp} = 0.3$ eV, and $t_{pp} = -t_{ss} = 0.2$ eV. For crossing bands, the sp interaction leads to band interaction, which in turn causes anti-crossing bands; meanwhile, non-crossing bands are weakly affected. When the SOC is turned on, bands with and without crossing respectively lead to small (B) and large (D) Rashba coefficients, giving the differentiation of the band dispersion of weak and strong Rashba effects.

proportional to the SOC (i.e., $\alpha_R = 2at_{soc}$), and decreases as the inter-orbital interaction increases, since orbitals are deformed by the atomic bonding.[41,42] However, for anti-crossing bands in TB, α_R and RSS depend on the inter-orbital coupling strength (an effect absent from Equation 1), as shown in Figure 4. We see that with weak inter-orbital interaction, α_R is much larger than the SOC itself ($\alpha_R = 4$ eVÅ for SOC of 0.5 eV) and the RSS also reach large values (here, 400 meV) (Figure 4). Both α_R and RSS decrease monotonically as the orbital interaction increases. For strong inter-orbital interaction, the α_R reaches a constant value corresponding with the Rashba effect without anti-crossing. The RSS tends to values smaller than 50 meV, showing that even for anti-crossing bands, while the Rashba parameter is large the RSS is not necessarily large.

DFT Validation of the Role of Band Anti-crossing in the Rashba Scale

As already noted, the TB model lacks material realism, but we can test via realistic DFT calculations the central insight it provides: we can directly detect in 3D DFT calculations with SOC which compound has band anti-crossing and distinguish it from compounds that lack band anti-crossing. This is done by orbital-projected band structure, i.e., calculating the weight of the atomic orbitals in the wave function for each k-point and each band index. Specifically, the qualitative different band shapes in TB depiction of compounds with large α_R (Figure 3D) and small α_R (Figure 3B) are linked to the realistic DFT depiction via the atomic orbital contributions to the band structures where band anti-crossing is directly identified by verifying the existence of orbital character change as the momentum goes from $k<k_R$ to $k>k_R$. We have studied
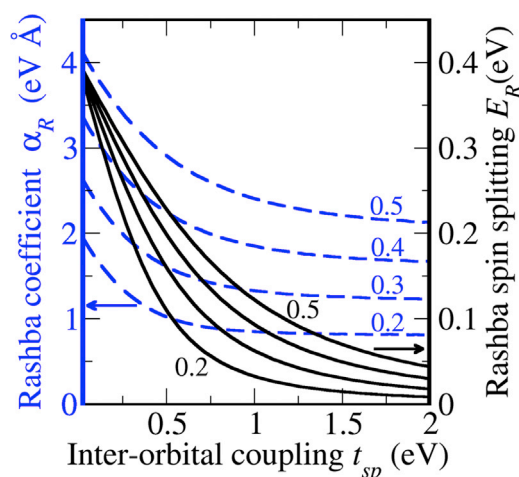
Figure 4. Variation of the Rashba Coefficient α_R (Dashed Blue Lines) and Rashba Spin Splitting (Solid Black Lines) as a Function of s-p Orbital Coupling for Anti-crossing Bands

Different values of the SOC are denoted for each blue line. Note that the variation of the RSS as a function of the band interaction is slower as the SOC increases.

the band crossing versus band anti-crossing behavior of the compounds shown in the survey (Figure 1).

We show in Figure 5 the DFT-calculated band shape and orbital-projected band structure predicted in Figure 1 to be strong Rashba compounds. For instance, in BiTeI (Figure 5A), for $k<k_R$, the Te-sp_z (Te-p_{xy}) orbital contributes to the VBM (conduction band minimum [CBM]), but for $k<k_R$, this orbital contribution moves to the CBM (VBM), as indicated by the magenta (green) dashed line. This indicates the existence of band anti-crossing. All DFT-confirmed strong Rashba compounds clearly show band anti-crossing (see orbital-projections for PbS, Sb2Se2Te, and GeTe in Figures 5B–5D). Thus, the DFT calculations are in agreement with the physical causal relation between the existence of anti-crossing bands and strong Rashba effect. This definition of the Rashba scale also provides a numerical description of the strong Rashba effect, i.e., all compounds with Rashba coefficient approximately larger than 1.3 and 1.6 eVÅ in the VBM and CBM (see Table 3), respectively, are also strong Rashba compounds. We term compounds with strong Rashba (i.e., large α_R and band anti-crossing) type I, whereas compounds with weak Rashba (i.e., small α_R and no anti-crossing) are type II.

The Emerging Cross-Functionality of Topological Rashba Insulators

We next explore some of the consequences of the aforementioned definition of the Rashba scale, i.e., that a type I Rashba compound can only be found in compounds also featuring energy band anti-crossing.

There is a class of material functionality that is characterized by always having energy band anti-crossing, namely TIs.[44] TIs have an inversion in order between valence and conduction bands; however, this does not guarantee the energy band anti-crossing (e.g., HgTe has inversion in band order even when calculated without SOC[45]). Band anti-crossing in TIs is only created if the interaction of the inverted bands is symmetry allowed,[46] whereas when the interaction between inverted energy bands is symmetry forbidden, the compound exhibited is a topological metal, not insulator.[47] Given that TI always has band anti-crossing and that strong Rashba compounds must have band anti-crossing, we next enquire as to what are the additional conditions for a TI to have RSS (so it would be a type I material).

We recall that the symmetry condition the Rashba R-1 effect[8] is that the compound must be non-centrosymmetric with a non-zero local electric dipole that add up over
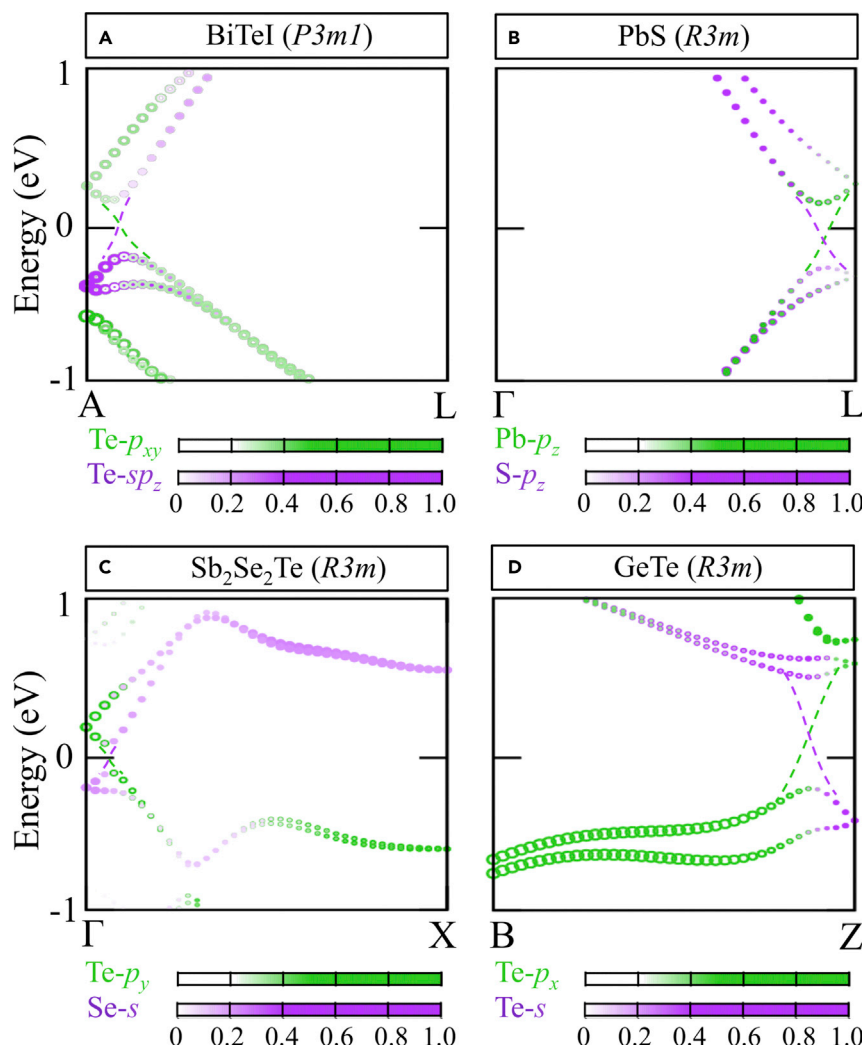
Figure 5. Orbital-Projected Band Structure for the Strong Rashba Materials
(A) BiTeI, (B) PbS, (C) Sb2Se2Te, and (D) GeTe (codes 74501, 183243, 60963, and 56040 in the Inorganic Crystal Structure Database,[43] respectively). The green and magenta color scales stand for the orbital contribution to the CBM and VBM at the time-reversal high-symmetry k-points, respectively. These orbital contributions change for momentums larger than the momentum offset, indicating the existence of anti-crossing bands. Only orbitals defining the anti-crossing are shown. The size of the dots also varies according to atomic orbital weight in the wavefunction of each k-point and band index. Dashed green and magenta lines are shown to guide the view to the change of the orbital character.

the unit cell to non-zero value. Thus, according to the proposed theory, all non-centrosymmetric TIs having local dipoles that add up to non-zero are strong Rashba compounds. This observation will be used below to explain previously puzzling observation of trends in Rashba effects in TIs and to identify compounds that have the cross-functional property of TIs while also being Rashba materials (TRIs).

Experimental evidence of trends in Rashba behavior in non-centrosymmetric TIs was observed in thin films of n formula units $(Bi_2Se_3)_n$ of the TI Bi_2Se_3 grown in a SiC substrate.[21] Figure 6 shows the experimentally estimated Rashba coefficient for different repeat units n in (Bi_2Se_3) plotted against the estimated effective electric potentials that reflects the breaking of inversion symmetry (generated here by the
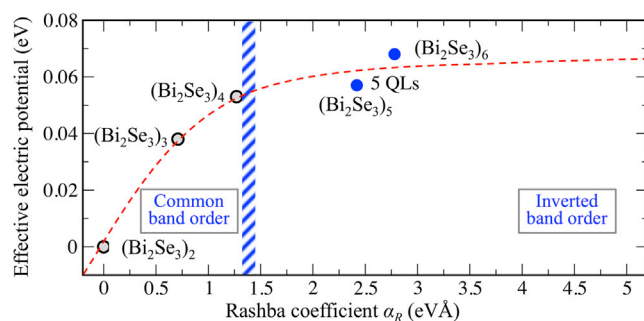
Figure 6. Variation of the Experimentally Estimated Rashba Coefficient α_R and Effective Electric Potential as a Function of the Slab Thickness in the Topological Insulator Bi_2Se_3

Slabs with common band order (non-topological insulators) and inverted band order are represented by the gray and blue dots, respectively. An abrupt change in the Rashba coefficient is observed when the band order changes. The blue hatched area (indicated also in Figure 1) separates slabs with different band order and small from large Rashba coefficients. The red dotted line shows the trends of the Rashba coefficient as function of the effective electric dipole (from Zhang et al.[21]).

induced electric dipole of SiC substrate). As seen in Figure 6, this electric potential changes when n increases, but it remains almost the same for $n = 4$ and $n = 5$, so both the SOC and the electric dipole are almost constant for these n values. This leaves unexplained the $\Delta\alpha_R = 1.15$ eVÅ jump in the Rashba coefficient between with $n = 4$ and $n = 5$ despite having the same SOC and potential asymmetry. This surprising fact is, however, in agreement with the band anti-crossing theory of the strong Rashba effect as Bi_2Se_3 thin films, as band inversion (and band anti-crossing) have been predicted to take place only for $(Bi_2Se_3)_n$ with $n > 4$,[21] as indicated in Figure 6. In other words, the inversion in the band structure is accompanied by an abrupt change in the Rashba coefficient $\Delta\alpha_R$.

The Way to Identify Topological Insulator Compounds that Are at the Same Time Rashba Materials

Finding cross-functionalities, such as multiferroics,[48,49] ferroelectrics that are Rashba,[50] transparent conducting compounds,[51–53] and electrical conductors that are thermal insulators, is always interesting.[54,55] TRIs will have spin-split surface states, an interesting yet unobserved behavior. The task of identifying compounds that are TIs and Rashba starts by finding TIs (steps a to c in Table 1) and then filtering out those TI that have at least one polar atomic site in the unit cell, and a non-zero total dipole (steps d to e in Table 1), i.e., that qualify as Rashba. According to the foregoing band anti-crossing theory, Rashba compounds that are TI must be strong Rashba compounds. Below we detail these steps:

(a) *Finding compounds that have their band structure computed by DFT + SOC.* We use literature databases[25–27] that were obtained by screening the Inorganic Crystal Structure Database[43] (ICSD), including now a total of 203,380 entries, However, to determine TI-ness of a compound, one needs[25] to compute its band structure including SOC. This requirement has drastically reduced the fraction of 203,000 ICSD compounds simply because for ~90% of ICSD compounds the calculation of the band structure was deemed problematic for one reason or another. The reasons (theoretical, computational, structural, financial) are different among different databases[25–27] and are summarized in Supplemental Information II. The results of these initial restrictions is (line a in Table 1) that Vergniory et al.[25] inspected 22,652 compounds

Table 1. Screening of Topological Rashba Materials

Filters	Vergniory et al.[25]	Tang et al.[26]	Wu et al.[27]
a. Shorter lists obtained from ICSD	22,652	19,143	13,628
b. Symmetry protected topological phases	7,385	1,075	4,050
c. Non-zero band gap	277	273	50
d. At least one polar atomic site	15	18	7
e. Non-zero dipole	0	0	3

The first filter is the initial restrictions that the repositories applied to the ICSD to find a shorter list for which calculations have been done. Subsequently, the applied filters select all TIs from these shorter lists; all compounds with band gap larger than 10^{-4} eV (non-zero band gap); compounds with at least one polar atomic site (i.e., polar space groups); and finally, compounds with non-zero total dipole.

as TI candidates, Tang et al.[26] inspected 19,143 compounds, while Wu et al.[27] inspected 13,628 compounds (see Table 1, line a).

(b) *Find the fraction of compounds that can be symmetry protected topological phases* (metals or insulators). Given these restricted lists of potential TIs, the literature has then applied filters guaranteeing compounds with symmetry indicators of topological phases, i.e., capable of having an inversion in the order of bands. This is based on the topological class defined in terms of "elementary band representations,"[44] symmetry indicator,[56] or topological invariant.[46] This filter leaves 7,385, 1,075, and 4,050 topological materials (either metals or non-metals) taken from Vergniory et al.,[25] Tang et al.,[26] and Wu et al.,[27] respectively (line b in Table 1).

(c) *Find the fraction of topological compounds that are topological insulators.* We then select compounds reported as non-metals (band gaps [E_g] larger than 10^{-4} eV), which results in a considerable reduction of the databases, i.e., 277, 273, and 50 TIs, respectively (line c in Table 1). We note that such tiny band gaps hardly qualify as "insulators" (despite the ubiquitous use of that term instead of "non-metals" to describe arbitrarily small band gaps). For example, inspection of the 277 nonmetallic topological compounds of Vergniory et al.[25] for those with a DFT gap of at least 0.1 eV or 0.5 eV leaves 34 and 0 topological narrow-gap semiconductors, respectively. The condition of non-zero band gap (line c in Table 1), which is not related to the Rashba effect but is required to guarantee anti-crossing bands, leads to an abrupt decrease in the yield of qualifying compounds. Interesting observations are that topological insulators are rather rare among the ICSD compounds examined (far more than, e.g., superconductors), and the vast majority of topological phases found are metals, being of less interest for physics that occurs inside the band gap, such as transport, Rashba effect, and topological surface states.

(d) *Find the fraction of TIs that are non-centrosymmetric.* To this end we select out of the compounds that are topological non-metals (step c) compounds with space groups having at least one polar atomic site. The list of point groups with at least one polar site is given in Figure S1 of Supplemental Information III. This leaves us in step d with 15, 18, and 7 compounds from lists of the respective databases[25–27] (line d in Table 1). We note that in such compounds with at least one polar atomic site the necessary electric dipole for the Rashba effect can still be zero. Thus, step (e) is needed.

(e) *Find the fraction with non-zero total dipole.* To guarantee Rashba-ness, the last applied filter distills compounds with non-zero total dipole (line e in Table 1). The existence of finite net dipole is determined by local asymmetric charge distributions that add up to non-zero. These local charges are induced by
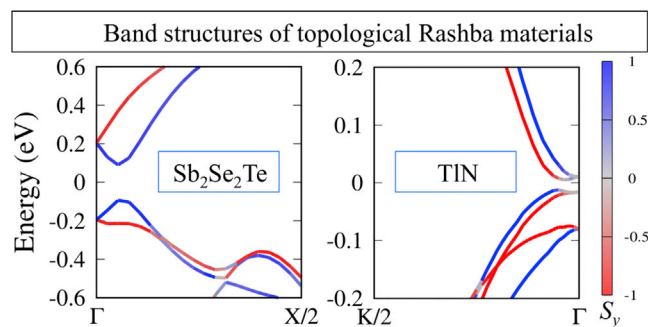
Figure 7. Band Structure of the Predicted Topological Rashba Sb_2TeSe_2 and TlN
The color scale stands for the expected values of the spin operator S_y.

inter-atomic bonding, which can be distributed in such a way that the dipole vectors generated by each bonding accidentally cancel each other (see Supplemental Information III). The three TI databases[25–27] leave only 0, 0, and 3 cross-functional TRI compounds, respectively: Sb_2TeSe_2, $K_5Fe_2O_6$, and TlN. Unfortunately, according to our own DFT band calculation, $K_5Fe_2O_6$ is more stable in a ferromagnetic configuration (with $E_{AFM} - E_{FM} = 2.7$ eV per formula), meaning that the time-reversal symmetry is not preserved, so it is not an R-1 compound. We tested our method of deduction by calculating in DFT the band anti-crossing and Rashba coefficient of Sb_2TeSe_2 and TlN in Figure 7.

DFT calculations for the screened compounds (Figure 7) verify that these are correctly predicted as strong Rashba semiconductors, as we discuss below. The two TI compounds Sb_2TeSe_2 ($R3m$)[57] and TlN ($P6_3mc$)[58] have been synthesized and predicted by our calculation to have a rather large Rashba parameter of 3.88 and 2.6 eVÅ for Sb_2TeSe_2 and TlN, respectively. The band structures of these compounds are shown in Figure 7. Both compounds are classified in Wu et al.[27] as topological insulators protected by the TR symmetry. Our calculated DFT band gaps are 179 meV and 18 meV for Sb_2TeSe_2 and TlN, respectively. This suggests that TlN is near a topological transition with a small spin splitting of 6 meV. The robust TIs Sb_2TeSe_2 has a very large spin splitting of 166 meV.

The interesting, albeit disappointing, result is that as we start from extensive lists of thousands of symmetry protected topological materials and then impose conditions for Rashba-ness, we find only two strong Rashba compounds (Sb_2TeSe_2 and TlN). This very small yield might suggest that perhaps "TI-ness" and "Rashba-ness" might be somehow contraindicated. More likely, however, is that the currently available list of TI with good insulating gap whose band structure has been calculated is very small: if a broader list of TIs compounds would be available (steps a and b in Table 1), more Rashba compounds with large coefficients might be identified: Note that the initial restrictions in step (a) to <10% of the known inorganic compounds could unfortunately exclude some important Rashba candidates (see Supplemental Information II). Furthermore, the condition of non-zero band gap (line c in Table 1) leads to small yield of only 2% (<277) of inorganic compounds that are TIs, and even fewer (34 compounds) if the minimum gap has to be 0.1 eV.

Most importantly, considering the condition of non-centrosymmetric TIs, the fraction is less than 0.1% of the initial shortened lists (e.g., only 15 NC-TIs in the list of 22,652 compounds of Vergniory et al.[25]). This means that the number of NC-TIs is

small in the reported lists, which is not related to existence of Rashba materials in nature. Indeed, we emphasize that these filters (band gap and NC space groups, lines c and d in Table 1) are not conditions for the specific selection of either weak or strong Rashba compounds. The highlight here is that all selected TRIs are predicted to be strong Rashba compounds, as predicted by the proposed definition of the Rashba scale as a consequence of the existence of energy band anti-crossing.

Discovery of Strong Rashba Compounds via DFT Prediction of Band Anti-crossing

The previous section looked for the interesting cross-functionality of TIs that are also Rashba compounds, starting from TIs and downselecting those that are Rashba like. The complementary search, ignored thus far, starts from Rashba compounds and downselects those that have anti-crossing bands even if they are not TIs. It turns out that the yield of this complementary search is much larger than that of the previous search.

As we will start from Rashba compounds, one needs to note that there are a few types of Rashba band splitting compounds: when the splitting is either between different valence bands, between different conduction bands, or between valence and conduction bands. For instance, as Figure 2A shows for KSn_2Se_4, the interaction between the valence bands Γ_{1v} and Γ'_{1v} along the Γ-X symmetry path is symmetry allowed, leading to a strong Rashba effect inside the valence bands. However, there is no anti-crossing between valence and conduction bands, so the Rashba effect at such a band edge is weak. Here, we are interested primarily in compounds featuring band edge Rashba splitting, i.e., near the VBM or CBM. To this end we will focus only on anti-crossing between these band edge states.

Figure 8 describes the selection strategy based on our design principles, which is divided into three filtering processes, shown in the vertical column in Figure 8. Supplemental Information III provides more technical details on the selection strategies. We consider a database of Rashba R-1 compounds, i.e., in which the inversion symmetry is broken by dipoles generated by intrinsic polar atomic sites (steps 1 and 2 below). Such a database has not existed as yet and will be constructed below. After this we will downselect those Rashba compounds that have band anti-crossing (step 3 below). Our 3 steps are as follows.

(1) *Find non-magnetic gapped compounds calculated previously by DFT* (filter 1 in Figure 8). Our starting point is the AFLOW-ICSD database (note that most compounds in ICSD have been previously synthesized),[59] containing 20,831 unique compounds with less than 20 atoms per unit cell that were calculated by DFT (see Experimental Procedures for details). Next, we downselect (filter 1 in Figure 8) those compounds that have time-reversal symmetry (non-magnetic) resulting in 13,838 non-magnetic compounds, from which 6,355 are gapped non-magnetic compounds (band gap larger than 1 meV). We note that the aforementioned database used as magnetic configuration a ferromagnetic ordering.

(2) *Find the subset of non-magnetic gapped compounds that has non-centrosymmetric space group with at least one polar atomic site and non-zero dipole* (filter 2 in Figure 8). We use the space group of the compounds to filter materials with polar atomic sites (polar space groups). The list of point groups with at least one polar site is given in Figure S1 of Supplemental Information III. The cancellation of dipoles can be geometrically determined for each atomic site by considering vectors along the atomic bonds (details of the
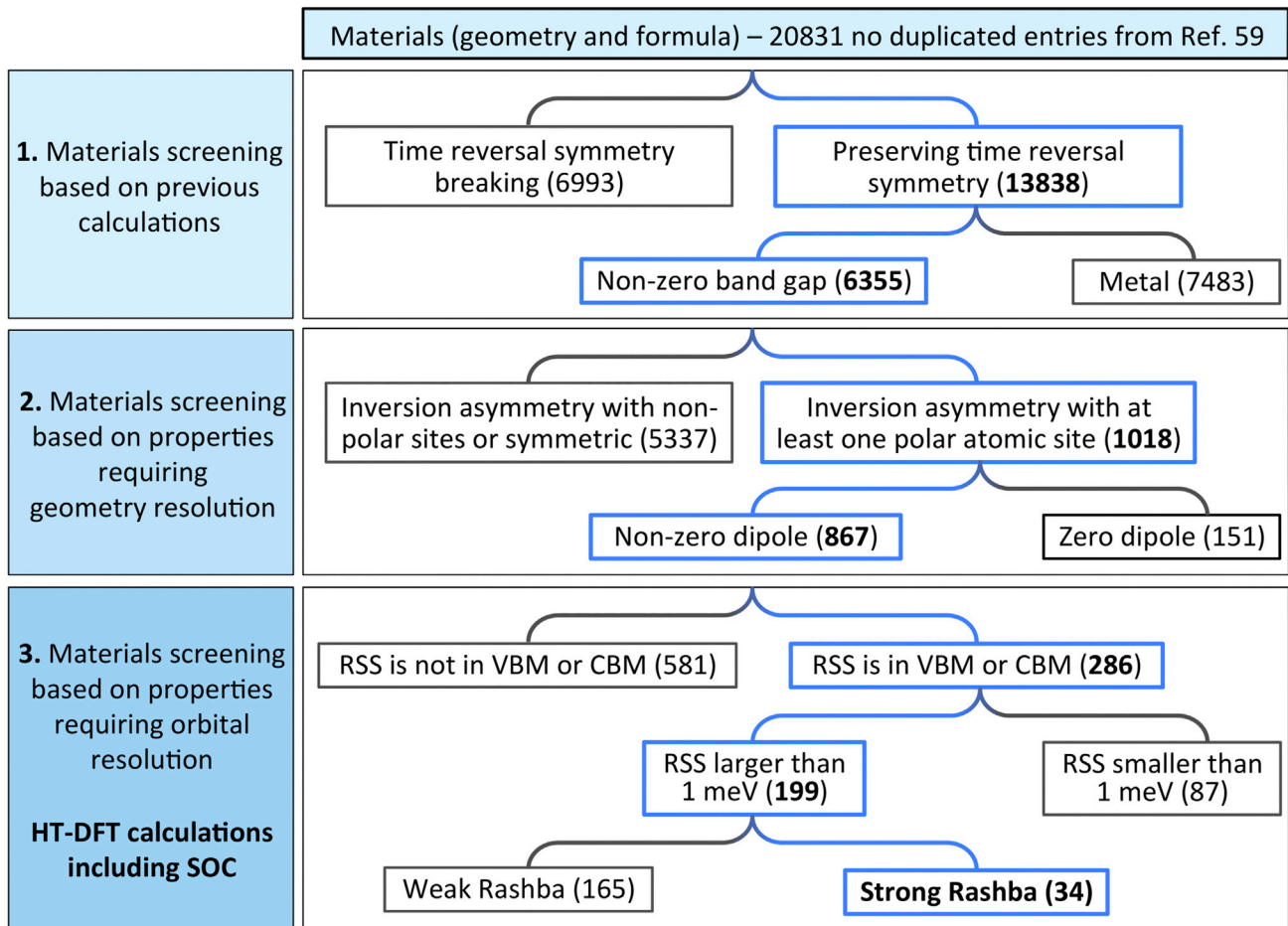
Figure 8. Schematic Representations of Filters Applied to Find Strong Rashba Material
These properties are separated in terms of the input required to compute them and also in terms of a binary selection that accept (blue) or reject (black) compounds.

cancellation of dipole can be found in Supplemental Information III). This gives 867 compounds that are Rashba non-metals.

(3) Sort out the subsets of Rashba non-metals with anti-crossing bands (type I Rashba) and with no anti-crossing bands (type II Rashba) (filter 3 in Figure 8). To do so we perform high-throughput DFT calculations including SOC of the band structure and spin texture for the 867 Rashba non-metals in order to identify anti-crossing bands and classify them into strong and weak Rashba compounds (DFT details are given in Experimental Procedures). We find 286 Rashba compounds with spin splitting positioned within 30 meV or less from the band edges, the rest having spin-split bands away from the band edges. Among these band edge Rashba insulators we find 199 that have non-negligible spin splitting of 1 meV or more.

We next apply to these compounds our orbital projection analysis of band anti-crossing versus no band anti-crossing (see Figure 4) to discern strong from weak effects. The distinction between anti-crossing and non-crossing bands (and hence between strong and weak Rashba effects) is evidenced by the change in the atomic orbitals weight in the wavefunction around the momentum offset k_R. Specifically, in non-crossing bands, the orbital character is essentially the same along all k-points

(see Figure 3B). However, for anti-crossing bands, the orbital character for *k*-vectors smaller and larger than the momentum offset is expected to be different (see Figure 3D). Additionally, the valence and conduction bands are made of different atomic orbitals (which are in different sites), as previously discussed. Using band anti-crossing, we identify for the final 199 selected Rashba compounds with spin splitting above 1 meV those having a strong Rashba effect. This leads to 165 weak and 34 strong Rashba compounds that have been previously synthesized, most of them unappreciated as Rashba materials.

DISCUSSION

Assessment of the Predicted Trends in Strong Rashba Compounds

We show that when the interaction between crossing bands is symmetry allowed, the induced anti-crossing leads to large RSS (strong Rashba compounds). We demonstrate that the anti-crossing is a design principle for the large Rashba coefficients in crystalline solids, in addition to the well-established necessary but insufficient conditions (NC space group, dipole generated by polar atomic sites, and the presence of SOC). Notable trends include:

(1) An immediate consequence of the aforementioned design principle is that when TIs satisfy the symmetry condition to be Rashba compounds they must have a strong Rashba effect because TI intrinsically have band anti-crossing. Because of limitations in the current listing of TI compounds,[25–27,60] we find only two positive predictions of strong TRIs (TlN and Sb_2Se_2Te).

(2) Based in our inverse design approach, we predict 13 previously synthesized but unnoticed as Rashba compounds with spin splitting in both VBM and CBM with large Rashba coefficient in at least one band (Table 2), nine Rashba compounds with spin splitting in both VBM and CBM with large Rashba coefficient in both bands (Table 3), nine compounds with strong Rashba effect in the CBM (Table 4), and an additional three compounds with strong Rashba effect in the VBM (Table 5). The Rashba parameters, as well as the spin splitting and momentum offset, are specified in Tables 2, 3, 4, and 5. Band structures and spin texture of the predicted compounds with larger Rashba coefficient are shown in Supplemental Information IV. Compounds with the same symmetry, atomic identities, and composition can have different format of the Rashba bands or position of the band edges due to different temperatures or fabrication methods. We exclude compounds with very similar RSS or Rashba coefficient, listing then in Tables 2, 3, 4, and 5 similar compounds with different RSS or band edges in different high-symmetry *k*-points. These are also identified by different ICSD codes.

(3) Considering the predicted compounds, we find cases that have a higher Rashba parameter than the largest currently known, e.g., 5.3 and 4.6 eVÅ for $K_2BaCdSb_2$ ($Pmc2_1$) and PbS ($R3m$), respectively. We also find giant RSS, even as large as the previously reported for GeTe and BiTeI. For instance, for Ga_2PbO_4 (Ama2), the RSS is about 144 meV. Bands with the same representation are a required condition for large RSS in BiTeI,[61] and the anti-crossing reveals the relation of this condition with the orbital character and orbital interactions.

(4) For direct-band-gap compounds, we find that the Rashba splitting for the VBM and CBM occurs at the same time-reversal symmetry invariant *k*-point. In this case, the momentum offset is the same for both VBM and CBM, as predicted in our model, e.g., PbS ($R3m$), KIO_3 ($R3m$), $K_2BaCdSb_2$ ($Pmc2_1$), and Sb_2Se_2Te ($R3m$). In general, the momentum offset is small, leading to large

Table 2. Rashba Compounds with Rashba Spin Splitting Both in VBM and in CBM and with Large Rashba Coefficient in at Least One of These Bands

Material	ICSD	SG index	K_v	E_{Rv}	k_{Rv}	α_{Rv}	K_c	E_{Rc}	k_{Rc}	α_{Rc}
$CsCuBi_2S_4$	93370	36	Γ	41.5	0.258	0.322	Y	48.2	0.034	2.864
SbF	30411	40	Y	3.1	0.056	0.109	Γ	175.3	0.124	2.836
KIO_3	97995	160	Z	17.4	0.055	0.628	Z	75.8	0.055	2.741
PbS	183249	28	X	1.7	0.035	0.099	Y	45.4	0.035	2.628
ZnI_2O_6	54086	4	Z	16.8	0.334	0.101	X	111.0	0.091	2.448
Ga_2PbO_4	80129	40	R	1.8	0.046	0.079	Y	144.4	0.119	2.428
IrSbS	74730	29	U	58.7	0.092	1.370	Γ	10.9	0.026	0.824
Ga_2PbO_4	33533	1	N	1.1	0.020	0.116	Y	142.8	0.119	2.398
$CsPbF_3$	93438	161	Γ	2.8	0.017	0.324	Γ	62.3	0.052	2.380
PbS	183250	28	X	1.2	0.034	0.071	Y	40.7	0.034	2.372
KIO_3	247719	146	Γ	8.2	0.057	0.288	Γ	62.0	0.057	2.185
KIO_3	424864	161	Γ	7.1	0.038	0.378	Γ	60.1	0.057	2.120
$PbTeO_3$	61343	76	X	11.6	0.133	0.175	M	38.2	0.044	1.721

For each compound, we present the ICSD code, space group (SG) index, high-symmetry k-point for the Rashba splitting in the valence (K_v) and conduction bands (K_c), Rashba spin splitting (E_{Rv} and E_{Rc}) in meV, momentum offset (k_{Rv} and k_{Rc}) in $\mathring{A}^{-1}$, and the Rashba parameters (α_{Rv} and α_{Rc}) in eV$\mathring{A}$.

Rashba parameters even when the RSS is not large. On the other hand, compounds with indirect band gap can exhibit RSS at different k-points, i.e., the position of the VBM and CBM. This leads to (a) compounds with RSS at different time-reversal symmetry points (Table 2) and (b) compounds with RSS at only one band edge (Tables 3 and 4). In this second group, the RSS is far from either the VBM or CBM; examples of this material include the KSnSb ($P6_3mc$) with RSS of 80 meV and Rashba parameter of 3.86 eVÅ in the CBM.

Conclusion

To form a broad view of design principles for large Rashba parameters in solids, we perform large-scale DFT calculations of more than 800 potential Rashba compounds. These calculations capture the physical mechanism determining the "Rashba scale," which is the basis of the proposed theory given here to explain and guide the selection of large Rashba compounds. Specifically, we show that when the interaction between crossing bands is symmetrically allowed, the induced anti-crossing leads to large RSS (strong Rashba compounds). We demonstrate that the anti-crossing is a design principle for the large Rashba coefficients in crystalline solids, in addition to the well-established necessary but insufficient conditions (NC space group and dipole generated by polar atomic sites). This establishes a causal relation between TIs and large Rashba coefficients, thus defining the cross-functionality of TRIs. We used the proposed design principles as filters to distill from a large set of compounds those featuring a strong Rashba effect. For instance, from lists of TIs, which intrinsically exhibit anti-crossing bands, filtering compounds with the aforementioned conditions find two positive predictions of strong Rashba compounds (TlN and Sb_2Se_2Te). In the same spirit, from the performed DFT calculations we filter compounds with anti-crossing bands, predicting 34 strong Rashba compounds, which include the known GeTe and BiTeI and the fabricated (but unnoticed as Rashba) compounds PbS ($R3m$), BiTeCl ($P6_3mc$), and $BaCdK_2Sb_2$ ($Pmc2_1$). These

Table 3. Strong Rashba Compounds with Rashba Spin Splitting Both in VBM and in CBM

Material	ICSD	SG index	K_v	E_{Rv}	k_{Rv}	α_{Rv}	K_c	E_{Rc}	k_{Rc}	α_{Rc}
BiTeI	74501	156	A	191.5	0.084	4.548	A	226.1	0.063	7.158
BiTeI	79364	156	A	187.9	0.084	4.475	A	218.8	0.063	6.948
Sb_2TeSe_2	60963	160	Γ	101.6	0.052	3.885	Γ	144.0	0.045	6.402
$K_2BaCdSb_2$	422272	26	Γ	18.6	0.016	2.356	Γ	41.5	0.016	5.251
PbS	183243	160	L	20.1	0.019	2.119	L	43.5	0.019	4.587
BiTeCl	79362	186	Γ	133.0	0.075	3.564	Γ	56.7	0.025	4.557
GeTe	659808	160	L	21.6	0.019	2.312	L	28.2	0.019	3.015
GeTe	188458	160	Z	142.5	0.068	4.219	L	25.0	0.019	2.686
GeTe	56040	160	Z	185.1	0.085	4.352	L	47.7	0.037	2.576

For each compound, we present the ICSD code, space group (SG) index, high-symmetry k-point for the Rashba splitting in the valence (K_v) and conduction bands (K_c), Rashba spin splitting (E_{Rv} and E_{Rc}) in meV, momentum offset (k_{Rv} and k_{Rc}) in $Å^{-1}$, and the Rashba parameters (α_{Rv} and α_{Rc}) in eVÅ.

identified compounds provide a platform for spin-conversion devices and the exploration of phenomena potentially hosted by Rashba compounds.

EXPERIMENTAL PROCEDURES

Density Functional Theory Calculations

The DFT band structure calculations were performed using the Perdew-Burke-Ernzerhof generalized gradient approximation (PBE)[62] exchange-correlation functional and the Hubbard on-site term[63,64] as implemented in the Vienna Ab-initio Simulation Package.[65,66] We use the theoretical structures predicted in the AFLOW-database[59] by initially setting the magnetic configuration as ferromagnetic and non-magnetic and then performing the internal energy minimization of the experimental structure in the ICSD.[43] Our calculations were performed by assuming a non-magnetic configuration in the structures previously reported by Curtarolo et al.[59] as non-magnetic. This could lead to some false-positive non-magnetic determinations, as Curtarolo et al.[59] decided whether a structure is magnetic or not on the basis of a limited range of trial magnetic configurations (usually only FM) performed usually only with soft exchange-correlation energy functional. All the specific settings of the calculations with SOC (e.g., cutoff energies, k-point sampling, effective U parameters) are the same as those used in Curtarolo et al.[59]

High-Throughput DFT Quantification of Rashba Coefficients

For linear RSS, α_R is given by the ratio between the energy splitting and the momentum offset, i.e., $\alpha_R = 2E_R/k_R$. However, the value of the Rashba coefficient could depend on the symmetry path in the Brillouin zone.[20] The orbital interaction, and hence the anti-crossing bands, can depend on the symmetry of the specific k-vector. However, we here report the Rashba coefficient at the VBM and CBM calculated along the symmetry directions connecting the high-symmetry k-points. Additional analyses are required to study the specific conditions leading to anisotropic Rashba effect in each of the reported compounds. In this work, the Rashba coefficient for Rashba bands near the VBM or CBM is determined following these steps: (1) we first identify TRIM points with spin splitting by looking at the energy difference of spin bands along the high-symmetry path in the Brillouin zone; (2) performing the derivative of the energy dispersion with respect to the momentum, we select those TRIM points with changes in the sign of the derivatives for the upper (lower) band in the valence (conduction) band; (3) if the spin splitting is near the VBM (CBM) or less (more) than 30 meV below (above) the VBM (CBM), we use the numerical value of

Table 4. Strong Rashba Compounds with Rashba Spin Splitting Only in the CBM

Material	SG index	ICSD	K_c	E_{Rc}	k_{Rc}	α_{Rc}
GeTe	160	659811	Z	46.8	0.019	4.949
KSnSb	186	33933	G	80.2	0.042	3.862
Bi_2CO_5	44	94740	Z	141.9	0.088	3.232
KSnAs	186	40815	G	39.2	0.025	3.079
$TlIO_3$	160	62106	Z	56.9	0.052	2.184
Tl_3SbS_3	160	603664	Z	89.9	0.083	2.169
$CsGeI_3$	160	62559	Z	26.7	0.027	1.946
AuCN	183	165175	L	23.1	0.026	1.781
$KCuBi_2S_4$	36	91297	Y	51.2	0.035	2.947

For each compound, we present the space group (SG) index, ICSD code, high-symmetry k-point for the Rashba splitting in the conduction bands (K_c), Rashba spin splitting (E_{Rc}) in meV, momentum offset (k_{Rc}) in $Å^{-1}$, and the Rashba parameters (α_{Rc}) in eVÅ.

the k-point in which the sign of the derivatives changes (i.e., the momentum offset k_R) and the value of the spin splitting (E_R) to compute the Rashba coefficient, i.e., $\alpha_R = 2E_R/k_R$. This procedure is performed in an automatic way for all DFT-calculated band structures.

Orbital Interaction in a One-Dimensional Model

We here describe in more detail the proposed model for a one-dimensional (1D) chain of atoms, with two sites in the unit cell, one containing an s-orbital and other a p-orbital, as presented in Figure 9. For simplicity, we consider that the 1D chain of atoms is along the x axis, which imposes that the interaction between s- and p_x-orbitals is different from zero and the interaction between s- and p_{yz}-orbitals is symmetry forbidden. In the TB Hamiltonian, the matrix elements are given by

$$[H(k)]_{jj'}^{\sigma\sigma'} = \varepsilon_j\delta_{jj'} + \sum_\nu t_{jj'}e^{ik\cdot R_\nu},$$

where j and σ are the orbital (s- or p_x) and spin indexes ($\uparrow$ or $\downarrow$), respectively. The considered hopping terms are the inter-site intra-orbital interaction (same orbital and same spin at different unit cells, i.e., $t_{ss}^{\sigma\sigma}$ and $t_{pp}^{\sigma\sigma}$), the on-site SOC (same orbital and different spin at different unit cells, i.e., $t_{ss}^{\uparrow\downarrow}$ and $t_{pp}^{\uparrow\downarrow}$), and the inter-atomic interaction ($t_{sp}^{\uparrow\downarrow}$) (see Figure 9). The latter corresponds to the interaction between bands with different atomic orbital characters, which we refer to hereafter as band interaction. Thus, the Hamiltonian can be written as

$$H(k) = \begin{pmatrix} H_s(k) & H_{sp}(k) \\ H_{sp}^\dagger(k) & H_p(k) \end{pmatrix},$$

where local Hamiltonian $H_p(k)$ describing the interaction between p-orbitals is given by

$$H_p(k) = \begin{pmatrix} -\varepsilon_p + 2t_{pp}^{\uparrow\uparrow}\cos(k_xa) & -i2t_{soc}^p\sin(k_xa) \\ i2t_{soc}^p\sin(k_xa) & -\varepsilon_p + 2t_{pp}^{\downarrow\downarrow}\cos(k_xa) \end{pmatrix}.$$

The breaking of the inversion symmetry is introduced by imposing that the SOC (i.e., the interaction between different spins $t_{pp}^{\uparrow\downarrow}$) satisfy the relation $t_{pp}^{\uparrow\downarrow}(r) \neq t_{pp}^{\uparrow\downarrow}(-r)$. Specifically, we consider that $t_{pp}^{\uparrow\downarrow}(r) = -t_{pp}^{\uparrow\downarrow}(-r) = -t_{soc}^P$. As shown in the above Hamiltonian $H_p(k)$, this approximation gives the off-diagonal matrix element $[H_p(k)]_{pp}^{\uparrow\downarrow} = t_{pp}^{\uparrow\downarrow}(a)e^{ika} + t_{pp}^{\uparrow\downarrow}(-a)e^{-ika} = -i2t_{soc}^P\sin(k_xa)$. This symmetry-based

Table 5. Strong Rashba Compounds with Rashba Spin Splitting Only in the VBM

Material	SG index	ICSD	K_v	E_{Rv}	k_{Rv}	α_{Rv}
Te_7As_5I	8	31877	Z	165.7	0.19	1.748
LiSbZn	186	642350	G	29.7	0.042	1.424
LiSbZn	186	42064	G	27.9	0.042	1.334

For each compound, we present the space group (SG) index, ICSD code, high-symmetry k-point for the Rashba splitting in the valence bands (K_v), Rashba spin splitting (E_{Rv}) in meV, momentum offset (k_{Rv}) in $\mathring{A}^{-1}$, and the Rashba parameters (α_{Rv}) in eV$\mathring{A}$.

approximation leads to the same results expected in a $k \cdot p$ model (e.g., the Hamiltonian in Equation 1) using the $L \cdot S$ term (i.e., the Rashba term $\alpha_R \sigma_y k_x$ in one-dimensional system), as we show below.

For $k \to 0$, considering that $t_{pp} = t_{pp}^{\uparrow\uparrow} = t_{pp}^{\downarrow\downarrow}$, this Hamiltonian results in a very simplified expression for the p-orbital interaction, namely,

$$H_p(k) \approx \begin{pmatrix} -\varepsilon_p + 2t_{pp} - t_{pp}a^2k_x^2 & -i2t_{soc}^p k_x a \\ i2t_{soc}^p k_x a & -\varepsilon_p + 2t_{pp} - t_{pp}a^2k_x^2 \end{pmatrix}.$$

This expression can be rewritten as $H_p(k) \approx \sigma_0(-\varepsilon_p + 2t_{pp} - t_{pp}a^2k_x^2) + 2at_{soc}^p(\sigma_y k_x)$. In quasi-2D compounds, the SOC gives an equivalent expression for the off-diagonal matrix elements, i.e., $2at_{soc}^p(\sigma_y k_x - \sigma_x k_y)$. This reproduces phenomenological Hamiltonian in Equation 1, which intrinsically leads to the weak Rashba effect (i.e., small Rashba coefficient). From the off-diagonal term $2at_{soc}^p(\sigma_y k_x - \sigma_x k_y)$, the Rashba parameter can easily identified as $\alpha_R = 2at_{soc}$. Here, the eigenvalues of $H_p(k)$ are given by $E_{p\pm}(k) = -\varepsilon_p + 2t_{pp} - t_{pp}a^2k_x^2 \pm \alpha_R|k_x|$, which intrinsically accounts for the RSS in weak Rashba compounds as given by Equation 1. According to our results, Equation 1 can describe the spin splitting in weak Rashba compounds, even in 3D materials (as shown KSn_2Se_4). The dependence of the Bulk Rashba effect in 3D compounds with respect to the inter-atomic orbital interaction is essentially given by the energy band anti-crossing, which is the metric defining the Rashba scale.

Analogously for interactions only between p-orbitals, we have $H_s(k) \approx \sigma_0(\varepsilon_s - 2t_{ss} + t_{ss}a^2k_x^2) - 2at_{soc}^s(\sigma_y k_x)$. Finally, the matrix $H_{sp}(k)$, without loss of generality, counts for the interaction between s-and p-orbitals with different spin, i.e.,

$$H_{sp}(k) = \begin{pmatrix} 0 & -i2t_{sp}^{\uparrow\downarrow}\sin(k_x a) \\ i2t_{sp}^{\uparrow\downarrow}\sin(k_x a) & 0 \end{pmatrix}.$$

For weak inter-orbital interaction, $t_{sp}^{\uparrow\downarrow}$ is smaller. In that case, the Hamiltonian $H(k)$ can approximately be treated as block diagonal, where blocks separately describe s- and p-orbitals, and hence the Rashba parameter is approximately given by $\alpha_R = 2at_{soc}$.

The crossing between bands meanly formed by s- and p-orbitals only depends on the relative on-site energy between orbitals $\Delta_{sp} = (\varepsilon_s - 2t_{ss}) - (\varepsilon_p - 2t_{pp})$ and the intra-orbital interaction t_{ss} and t_{pp}. For instance, for $t_{ss} = t_{pp}$, bands cross when $\Delta_{sp} < 0$. The role of the inter-orbital interaction $t_{sp}^{\uparrow\downarrow}$ is to open the band gap, which increases as this interaction increases. For this reason, strong Rashba semiconductors (compounds exhibiting anti-crossing) usually also have smaller band gaps. In general, band anti-crossing can be designed in a periodic Hamiltonian by requiring a non-zero interaction between at least two different atomic orbitals

Tight-binding model
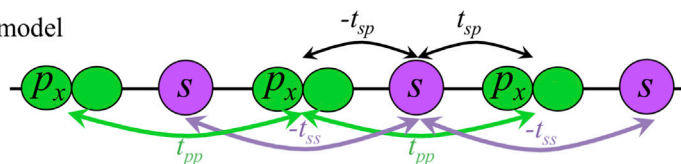
Figure 9. The TB Model: One-Dimensional Chain Formed by *s* (Magenta) and *p_x* (Green) Orbitals in Different Sites

The inter-orbital interaction t_{sp} and intra-orbital interactions t_{ss} and t_{pp} are schematically defined.

with opposite effective mass, as illustrated in the proposed 1D chain with two atomic species.

Note that we used here the *s*-orbitals as notation for states with total angular momentum equal to $J = 1/2$, and hence the discussion previously presented is for instance also extended to p_z-orbitals, which leads to a non-zero SOC. The pure *s*-orbitals should result in a zero RSS, since the SOC is zero. In fact, the obtained Hamiltonian $H(k)$ is similar to that discussed in Acosta and Fazzio[12] for the interaction between states with total angular momentum $J = 1/2$ and $J = 3/2$.

Resource Availability

Lead Contact

Alex Zunger. Email address: alex.zunger@colorado.edu.

Materials Availability

This study did not generate new unique reagents.

Data and Software Availability

All data needed to evaluate the conclusions in the paper are present in the paper and the Supplemental Information. Additional data related to this paper may be requested from the authors.

SUPPLEMENTAL INFORMATION

Supplemental Information can be found online at https://doi.org/10.1016/j.matt.2020.05.006.

AUTHOR CONTRIBUTIONS

All authors participated in the conceptual development of the project. C.M.A. and E.O. performed the calculations. C.M.A. and A.Z. conducted the analysis of the results and wrote the paper with input from all authors. A.Z., A.F., and G.M.D. directed the study.

REFERENCES

1. Manchon, A., Koo, H.C., Nitta, J., Frolov, S.M., and Duine, R.A. (2015). New perspectives for Rashba spin-orbit coupling. Nat. Mater. *14*, 871–882.

2. S. Maekawa, S.O. Valenzuela, E. Saitoh, and T. Kimura, eds. (2017). Spin Current, Second Edition (Oxford University Press).

3. Žutić, I., Fabian, J., and Das Sarma, S. (2004). Spintronics: fundamentals and applications. Rev. Mod. Phys. *76*, 323–410.

4. Rashba, E.I., and Sheka, V.I. (1959). Simmetriya energeticheskikh zon v kristallakh tipa vyurtsita. II. Simmetriya zon s uchyotom spinovykh vzaimodeistvii. Fizika tverd. tela. Collected Pap. (Leningrad) *1* (2), 162–176.

5. Rashba, E.I. (1960). Svoistva poluprovodnikov s petlei ekstremumov. I. Tsiklotronnyi i kombinirovannyi rezonans v magnitnom pole, perpendikulyarnom ploskosti petli. Fizika Tverd. Tela *2*, 1224–1238.

6. Bychkov, Yu.A., and Rashba, E.I. (1984). Properties of a 2D electron gas with lifted spectral degeneracy. JETP Lett. *39*, 78.

7. Vajna, Sz., Simon, E., Szilva, A., Palotas, K., Ujfalussy, B., and Szunyogh, L. (2012). Higher-order contributions to the Rashba-Bychkov effect with application to the Bi/Ag(111) surface alloy. Phys. Rev. B *85*, 075404.

8. Zhang, X., Liu, Q., Luo, J.-W., Freeman, A.J., and Zunger, A. (2014). Hidden spin polarization in inversion-symmetric bulk crystals. Nat. Phys. *10*, 387–393.

9. Yuan, L., Liu, Q., Zhang, X., Luo, J.-W., Li, S.-S., and Zunger, A. (2019). Uncovering and tailoring hidden Rashba spin-orbit splitting in centrosymmetric crystals. Nat. Commun. *10*, 906.

10. Datta, S., and Das, B. (1990). Electronic analog of the electro-optic modulator. Appl. Phys. Lett. *56*, 665–667.

11. Koo, H.C., Kwon, J.H., Eom, J., Chang, J., Han, S.H., and Johnson, M. (2009). Control of spin precession in a spin-injected field effect transistor. Science *325*, 1515–1518.

12. Acosta, C.M., and Fazzio, A. (2019). Spin-polarization control driven by a rashba-type effect breaking the mirror symmetry in two-dimensional dual topological insulators. Phys. Rev. Lett. *122*, https://doi.org/10.1103/PhysRevLett.122.036401.

13. Debray, P., Rahman, S.M.S., Wan, J., Newrock, R.S., Cahay, M., Ngo, A.T., Ulloa, S.E., Herbert, S.T., Muhammad, M., and Johnson, M. (2009). All-electric quantum point contact spin-polarizer. Nat. Nanotechnol. *4*, 759–764.

14. Mourik, V., Zuo, K., Frolov, S.M., Plissard, S.R., Bakkers, E.P.A.M., and Kouwenhoven, L.P. (2012). Signatures of majorana fermions in hybrid superconductor-semiconductor nanowire devices. Science *336*, 1003–1007.

15. Sato, M., and Fujimoto, S. (2009). Topological phases of noncentrosymmetric superconductors: edge states, Majorana fermions, and non-Abelian statistics. Phys. Rev. B *79*, 094504.

16. Di Sante, D., Barone, P., Bertacco, R., and Picozzi, S. (2013). Electric control of the giant rashba effect in bulk GeTe. Adv. Mater. *25*, 509–513.

17. Liebmann, M., Rinaldi, C., Di Sante, D., Kellner, J., Pauly, C., Wang, R.N., Boschker, J.E., Giussani, A., Bertoli, S., Cantoni, M., et al. (2016). Giant rashba-type spin splitting in ferroelectric GeTe(111). Adv. Mater. *28*, 560–565.

18. Ishizaka, K., Bahramy, M.S., Murakawa, H., Sakano, M., Shimojima, T., Sonobe, T., Koizumi, K., Shin, S., Miyahara, H., Kimura, A., et al. (2011). Giant Rashba-type spin splitting in bulk BiTeI. Nat. Mater. *10*, 521–526.

19. Sakano, M., Miyawaki, J., Chainani, A., Takata, Y., Sonobe, T., Shimojima, T., Oura, M., Shin, S., Bahramy, M.S., Arita, R., et al. (2012). Three-dimensional bulk band dispersion in polar BiTeI with giant Rashba-type spin splitting. Phys. Rev. B *86*, 085204.

20. Feng, Y., Jiang, Q., Feng, B., Yang, M., Xu, T., Liu, W., Yang, X., Arita, M., Schwier, E.F., Shimada, K., et al. (2019). Rashba-like spin splitting along three momentum directions in trigonal layered PtBi$_2$. Nat. Commun. *10*, 4765.

21. Zhang, Y., He, K., Chang, C.-Z., Song, C.-L., Wang, L.-L., Chen, X., Jia, J.-F., Fang, Z., Dai, X., Shan, W.-Y., et al. (2010). Crossover of the three-dimensional topological insulator Bi$_2$Se$_3$ to the two-dimensional limit. Nat. Phys. *6*, 584–588.

22. King, P.D.C., Hatch, R.C., Bianchi, M., Ovsyannikov, R., Lupulescu, C., Landolt, G., Slomski, B., Dil, J.H., Guan, D., Mi, J.L., et al. (2011). Large tunable rashba spin splitting of a two-dimensional electron gas in Bi$_2$Se$_3$. Phys. Rev. Lett. *107*, 096802.

23. Rauch, T., Flieger, M., Henk, J., and Mertig, I. (2013). Nontrivial interface states confined between two topological insulators. Phys. Rev. B *88*, 245120.

24. Mera Acosta, C., Babilonia, O., Abdalla, L., and Fazzio, A. (2016). Unconventional spin texture in a noncentrosymmetric quantum spin Hall insulator. Phys. Rev. B *94*, 041302.

25. Vergniory, M.G., Elcoro, L., Felser, C., Regnault, N., Bernevig, B.A., and Wang, Z. (2019). A complete catalogue of high-quality topological materials. Nature *566*, 480–485.

26. Tang, F., Po, H.C., Vishwanath, A., and Wan, X. (2019). Comprehensive search for topological materials using symmetry indicators. Nature *566*, 486–489.

27. Wu, Q., Autès, G., Mounet, N., and Yazyev, O.V. (2019). TopoMat: a database of high-throughput first-principles calculations of topological materials. https://archive.materialscloud.org/2019.0019/v1.

28. Zunger, A. (2018). Inverse design in search of materials with target functionalities. Nat. Rev. Chem. *2*, 0121.

29. Noh, J., Kim, J., Stein, H.S., Sanchez-Lengeling, B., Gregoire, J.M., Aspuru-Guzik, A., and Jung, Y. (2019). Inverse design of solid-state materials via a continuous representation. Matter *1*, 1370–1384.

30. Piquini, P., Graf, P.A., and Zunger, A. (2008). Band-gap design of quaternary (In,Ga)(As,Sb) semiconductors via the inverse-band-structure approach. Phys. Rev. Lett. *100*, 186403.

31. Yang, J., Zhang, S., Li, L., Wang, A., Zhong, Z., and Chen, L. (2019). Rationally designed high-performance spin filter based on two-dimensional half-metal Cr$_2$NO$_2$. Matter *1*, 1304–1315.

32. Curtarolo, S., Hart, G.L.W., Nardelli, M.B., Mingo, N., Sanvito, S., and Levy, O. (2013). The high-throughput highway to computational materials design. Nat. Mater. *12*, 191–201.

33. Woods-Robinson, R., Han, Y., Mangum, J.S., Melamed, C.L., Gorman, B.P., Mehta, A., Persson, K.A., and Zakutayev, A. (2019). Combinatorial tuning of structural and optoelectronic properties in Cu$_x$Zn$_{1-x}$S. Matter *1*, 862–880.

34. Schleder, G.R., Padilha, A.C.M., Acosta, C.M., Costa, M., and Fazzio, A. (2019). From DFT to machine learning: recent approaches to materials science—a review. J. Phys. Mater. *2*, 032001.

35. Moghadam, P.Z., Rogge, S.M.J., Li, A., Chow, C.-M., Wieme, J., Moharrami, N., Aragones-Anglada, M., Conduit, G., Gomez-Gualdron, D.A., Van Speybroeck, V., et al. (2019). Structure-mechanical stability relations of metal-organic frameworks via machine learning. Matter *1*, 219–234.

36. Schleder, G.R., Acosta, C.M., and Fazzio, A. (2019). Exploring two-dimensional materials

Thermodynamic stability via machine learning. ACS Appl. Mater. Interfaces, acsami.9b14530.

37. Krempaský, J., Muff, S., Bisti, F., Fanciulli, M., Volfová, H., Weber, A.P., Pilet, N., Warnicke, P., Ebert, H., Braun, J., et al. (2016). Entanglement and manipulation of the magnetic and spin–orbit order in multiferroic Rashba semiconductors. Nat. Commun. 7, 13071.

38. Mera Acosta, C., Fazzio, A., and Dalpian, G.M. (2019). Zeeman-type spin splitting in nonmagnetic three-dimensional compounds. NPJ Quan. Mater. 4, 41.

39. Rashba, E.I. (1960). Properties of semiconductors with an extremum loop. I. Cyclotron and combinational resonance in a magnetic field perpendicular to the plane of the loop. Soviet Phys. Solid State 2, 1109–1122.

40. Martin, W.C. (1971). Table of spin-orbit energies for p-electrons in neutral atomic (core) np configurations. J. Res. Natl. Bur. Stan. Sect. A. 75A, 109.

41. Ast, C.R., and Gierz, I. (2012). s p-band tight-binding model for the Bychkov-Rashba effect in a two-dimensional electron system including nearest-neighbor contributions from an electric field. Phys. Rev. B 86, 085105.

42. Petersen, L., and Hedegård, P. (2000). A simple tight-binding model of spin-orbit splitting of sp-derived surface states. Surf. Sci. 459, 49–56.

43. Crystallography: Inorganic Crystal Structure Database, University of California San Diego. https://ucsd.libguides.com/crystallography/icsd.

44. Bradlyn, B., Elcoro, L., Cano, J., Vergniory, M.G., Wang, Z., Felser, C., Aroyo, M.I., and Bernevig, B.A. (2017). Topological quantum chemistry. Nature 547, 298–305.

45. Wei, S.-H., and Zunger, A. (1987). Role of d orbitals in valence-band offsets of common-anion semiconductors. Phys. Rev. Lett. 59, 144–147.

46. Bansil, A., Lin, H., and Das, T. (2016). Colloquium: topological band theory. Rev. Mod. Phys. 88, 021004.

47. Armitage, N.P., Mele, E.J., and Vishwanath, A. (2018). Weyl and Dirac semimetals in three-dimensional solids. Rev. Mod. Phys. 90, 015001.

48. Fiebig, M., Lottermoser, T., Meier, D., and Trassin, M. (2016). The evolution of multiferroics. Nat. Rev. Mater. 1, 16046.

49. Hill, N.A. (2000). Why are there so few magnetic ferroelectrics? J. Phys. Chem. B 104, 6694–6709.

50. Picozzi, S. (2014). Ferroelectric Rashba semiconductors as a novel class of multifunctional materials. Front. Phys. 2, https://doi.org/10.3389/fphy.2014.00010.

51. Zhang, X., Zhang, L., Perkins, J.D., and Zunger, A. (2015). Intrinsic transparent conductors without doping. Phys. Rev. Lett. 115, 176602.

52. Yan, F., Zhang, X., Yu, Y.G., Yu, L., Nagaraja, A., Mason, T.O., and Zunger, A. (2015). Design and discovery of a novel half-Heusler transparent hole conductor made of all-metallic heavy elements. Nat. Commun. 6, 7308.

53. Brunin, G., Ricci, F., Ha, V.-A., Rignanese, G.-M., and Hautier, G. (2019). Transparent conducting materials discovery using high-throughput computing. NPJ Comput. Mater. 5, 63.

54. Cahill, D.G., Watson, S.K., and Pohl, R.O. (1992). Lower limit to the thermal conductivity of disordered crystals. Phys. Rev. B 46, 6131–6140.

55. Chiritescu, C., Cahill, D.G., Nguyen, N., Johnson, D., Bodapati, A., Keblinski, P., and Zschack, P. (2007). Ultralow thermal conductivity in disordered, layered WSe_2 crystals. Science 315, 351–353.

56. Po, H.C., Vishwanath, A., and Watanabe, H. (2017). Symmetry-based indicators of band topology in the 230 space groups. Nat. Commun. 8, 50.

57. Andriamihaja, A., Ibanez, A., Jumas, J.C., Olivier Fourcade, J., and Philippot, E. (1985). Evolution structurale de la solution solide $Sb_2Te(3-x)Se(x)$ (O < X < 2) dans le systeme Sb_2Te_3-Sb_2 Se_3. Revue de Chim. Minerale 22, 357–368.

58. Shaginyan, L.R. (2019). Synthesis and properties of thallium nitride films. Mater. Chem. Phys. 227, 157–162.

59. Curtarolo, S., Setyawan, W., Hart, G.L.W., Jahnatek, M., Chepulskii, R.V., Taylor, R.H., Wang, S., Xue, J., Yang, K., Levy, O., et al. (2012). AFLOW: an automatic framework for high-throughput materials discovery. Comput. Mater. Sci. 58, 218–226.

60. Malyi, O.I., Dalpian, G.M., Zhao, X.-G., Wang, Z., and Zunger, A. (2020). Realization of predicted exotic materials: the burden of proof. Mater. Today 32, 35–45.

61. Bahramy, M.S., Arita, R., and Nagaosa, N. (2011). Origin of giant bulk Rashba splitting: application to BiTeI. Phys. Rev. B 84, 041202.

62. Perdew, J.P., Burke, K., and Ernzerhof, M. (1996). Generalized gradient approximation made simple. Phys. Rev. Lett. 77, 3865–3868.

63. Liechtenstein, A.I., Anisimov, V.I., and Zaanen, J. (1995). Density-functional theory and strong interactions: orbital ordering in Mott-Hubbard insulators. Phys. Rev. B 52, R5467–R5470.

64. Dudarev, S.L., Botton, G.A., Savrasov, S.Y., Humphreys, C.J., and Sutton, A.P. (1998). Electron-energy-loss spectra and the structural stability of nickel oxide: an LSDA+U study. Phys. Rev. B 57, 1505–1509.

65. Kresse, G., and Furthmüller, J. (1996). Efficient iterative schemes for ab initio total-energy calculations using a plane-wave basis set. Phys. Rev. B 54, 11169–11186.

66. Kresse, G., and Joubert, D. (1999). From ultrasoft pseudopotentials to the projector augmented-wave method. Phys. Rev. B 59, 1758–1775.